Journal of Energy Storage 65 (2023) 107228

Contents lists available at ScienceDirect

Journal of Energy Storage

journal homepage: www.elsevier.com/locate/est

Research Papers

Influence of reversible swelling and preload force on the failure behavior of a lithium-ion pouch cell tested under realistic boundary conditions

Patrick Höschele [a,*], Simon F. Heindl [a], Simon Erker [b], Christian Ellersdorfer [a]

[a] Vehicle Safety Institute, Graz University of Technology, Inffeldgasse 23/I, Graz 8010, Austria
[b] AVL List GmbH, Hans-List-Platz 1, Graz 8020, Austria

ARTICLE INFO

Keywords:
Lithium-ion batteries
Pouch cell
Mechanical abuse
Out-of-plane
Preload force
Swelling

ABSTRACT

Safety of lithium-ion batteries plays an important role in the context of advancing electrification for vehicles. Pouch cells suffer from low structural strength and are often constrained within a battery module to guarantee mechanical integrity. The effect of constraints and SOC-dependent changes on the mechanical abuse behavior was not sufficiently investigated.

A total number of 36 pouch cells were indented with a flat-end cylinder under different boundary conditions until mechanical failure and thermal runaway occurred. The pouch cells were constrained at 30 % SOC with a preload force of 0, 300 or 4000 N and charged to 0 %, 30 %, 60 % or 100 % SOC before indentation.

The maximum indentation force, corresponding indentation, initial stiffness and failure behavior indicated a dependency on the preload force. The stiffness at greater indentation was similar for all boundary conditions indicating a pre-compression and flattening of unevenness. Internal stress within the separator resulted in earlier short circuit and mechanical failure for increasing preload force. The mechanical constraint led to increased gas pressure during thermal runaway.

The results in this publication give rise to an additional consideration of preload force and boundary conditions imposed by a battery module in abuse testing and simulation approaches in the future.

1. Introduction

Lithium-ion batteries (LIB) are the main component for the advancing electrification in the automotive sector and the advantages associated with the technology [1]. LIBs have inherent safety-relevant hazards such as a thermal runaway (TR) [2] and fire or explosion [3,4] when subjected to mechanical loads like deformations occurring during a crash [5–7] and resulting thermal propagation [8,9]. The safety performance on battery cell level in electric vehicles (EV) can be evaluated with the European Council for Automotive Research and Development (EUCAR) hazard levels during abuse testing to guarantee safe operation within an EV.

Different certification standards define mechanical abuse loads in order to determine the mechanical and failure behavior of LIBs and to derive the resulting hazard level [10,11]. The certification standards mostly neglect boundary conditions for mechanical abuse tests on cell level. Apart from certification standards, several investigations on different influencing factors affecting the mechanical and failure behavior of LIB cells can be found in the literature. The influencing factors include the loading rate, loading direction, state of charge (SOC), indenter geometry, temperature, aging, mechanical boundary conditions or cell type.

Zhu et al. [7], Liu et al. [12] and Kermani and Sahraei [13] reviewed mechanical abuse tests, relevant influencing factors and battery failure mechanisms under mechanical abuse conditions. Six loading conditions were mostly described in the literature. These were pinch tests, hemispherical punch, out-of-plane compression, in-plane compression, cylindrical punch and 3-point bending.

Many of the reported mechanical abuse tests were conducted with simplifications to reduce complexity of the test procedure and test setups. One simplification made is mechanical abuse testing on single LIB cells without realistic geometric boundary conditions. This simplification neglects the mechanical constraints of the LIB imposed by the battery module. Mechanical abuse tests on battery module level consider

Abbreviations: CC-CV, Constant current constant voltage; EUCAR, European Council for Automotive Research and Development; EV, Electric vehicle; ISC, Internal short circuit; LIB, Lithium-ion battery; SEI, Solid electrolyte interface; SOC, State of charge; TR, Thermal runaway.

* Corresponding author.
E-mail address: patrick.hoeschele@tugraz.at (P. Höschele).

https://doi.org/10.1016/j.est.2023.107228
Received 16 November 2022; Received in revised form 3 March 2023; Accepted 21 March 2023
Available online 7 April 2023
2352-152X/© 2023 The Authors. Published by Elsevier Ltd. This is an open access article under the CC BY license (http://creativecommons.org/licenses/by/4.0/).

geometric boundary conditions but imply complexity and superposition of different effects such as complex contact conditions with friction or mutual influence of battery cells during testing [14–16]. Geometric boundary conditions are especially relevant for pouch-type cells as this battery format suffers from lower structural strength and integrity in comparison to e.g. prismatic metal can cells [17].

Pouch cells are usually constrained at begin-of-life inside a battery module with a preload force to achieve mechanical integrity and improve cyclic lifetime [18–20]. Reversible swelling leads to cyclic thickness changes of pouch cells during charging and discharging by intercalation and deintercalation of lithium ions into the host materials [21–23]. Reversible swelling is therefore mainly dependent on the SOC. Aging mechanisms such as solid electrolyte interface (SEI) growth lead to irreversible swelling and a permanent thickness increase [18,24,25]. Thickness variations caused by reversible and irreversible swelling result in a SOC- and lifetime-dependent preload force on constrained pouch cells as the mechanical constraints constitute a resistance to the thickness increase of the pouch cell [20,26]. The mechanical resistance is determined by the battery module construction and the design elements used. Pouch cells are usually embedded between compression pads (e.g. soft Polyurethane) or flexible bracing to improve lifetime by accounting for thickness variations and the resulting mechanical load variations during battery lifetime [20,27–30].

Apart from lifetime, the interaction between the mechanical constraint and reversible and irreversible thickness changes lead to safety-relevant implications. Variations in mechanical loads affect the internal stress acting on components inside a pouch cell. As an example, compaction of the porous separator structure and resulting internal stress directly affects the failure behavior [31,32]. Several mechanical abuse tests with constrained pouch cells or parts of the jelly roll were performed in the thickness direction (out-of- plane) [33] and perpendicular to the thickness direction of the battery cell (in-plane) [34–38].

Cylindrical cells indicated a strong SOC-dependence on mechanical properties for different abuse load conditions including cylindrical punch [33,39], hemispherical punch [39,40] or radial compression [39–41]. It is assumed that the observed SOC-dependence on mechanical properties results from internal stress caused by an anode thickness increase upon charging. The expansion of the jelly roll is restricted by the housing of the cylindrical cells and the jelly roll gap reduces when the cylindrical cell is charged [42].

Several researchers investigated the possible SOC-dependency of the mechanical properties of prismatic battery cells. Internal stress can be expected to result in SOC-dependence on mechanical properties as observed for cylindrical cells as the prismatic battery cells also have a metal housing. However, Kotter et al. [43] did not observe a strong SOC-dependence of the mechanical properties, hardening and failure parameters for prismatic battery cells. Other researchers conducted experiments with prismatic battery cells and found SOC-dependent mechanical properties especially for the out-of-plane direction [38,44].

Li et al. [33] performed out-of-plane abuse tests with constrained pouch cells to prove that the metal can of cylindrical cells is causing internal stress when the battery cell is charged. In this work, the mechanical behavior of a constrained pouch cell was affected by the applied boundary condition and the pouch cells indicated a strong dependence on the applied preload force. Additionally, the constraining procedure affected the mechanical response of the pouch cells. Bolts were used to apply a preload force that resulted in stiff bracing of the pouch cells. Unconstrained pouch cells did not indicate a SOC-dependency of mechanical properties for a hemispherical indentation [45]. This can be attributed to the fact that the soft pouch foil is not restricting the thickness increase as much as a metal can case. In the case of pouch cells, the SOC-dependent thickness changes will therefore not create internal stress affecting the mechanical properties. Qu et al. [46] found a SOC-dependency of the mechanical response for three-point bending tests with unconstrained pouch cells. The authors assume that this SOC-dependency is a result of the interfaces between current collectors and the anode coating that change their properties when the battery cell is charged. The observed change in mechanical properties can also be explained by SOC-dependent material properties existing on the electrode level. A lithiated graphite electrode showed a higher Young's modulus [47] and an earlier failure in tensile tests [48].

Zhu et al. [36] constrained pouch cells with compression pads or bolts and performed in-plane abuse tests. The mechanical properties of the pouch cells indicated a dependence on the mechanical constraint. A compliant mechanical constraint caused a different deformation pattern compared to a stiff mechanical constraint.

In summary, the mechanical properties and the failure behavior of pouch-type LIBs depends on the boundary conditions like the mechanical constraint. Additionally, reversible and irreversible swelling have to be considered as the corresponding geometry changes affect the preload force of a constrained pouch cell. The mechanical constraint is expected to cause internal stress and have a similar effect as the metal can housing of cylindrical and prismatic cells. In a battery module, compression pads account for SOC- and lifetime-dependent geometry changes of pouch cells. A compliant mechanical constraint must be realized in order to test a pouch cell under realistic boundary conditions. Influencing factors like the applied preload force and the stiffness of the overall mechanical system need to be considered to allow for a safe mechanical integration of pouch cells within a battery module. The electro-mechanical failure behavior of constrained pouch cells has not yet been sufficiently investigated for a combination of different preload force levels, realistic mechanical constraints (soft – comparable to compression pads) and SOC-dependent geometry variations during out-of-plane indentation tests. An innovative test setup was designed to perform quasi-static out-of-plane mechanical abuse tests with pouch cells under realistic boundary conditions and in a repeatable way in order to fill the gap in literature.

The following research questions will be answered in this manuscript:

- To what extent does the preload force and SOC-dependent geometry variations (reversible swelling) influence the mechanical properties of a pouch cell during out-of-plane indentation?
- Is the failure behavior of a pouch cell during an out-of-plane indentation affected by the preload force and SOC-dependent geometry variations (reversible swelling)?

2. Method

The effect of a preload force and SOC on the mechanical response of lithium-ion pouch cells during quasi-static indentation tests was examined in this study. Furthermore, the effect of reversible swelling and the related change of thickness was investigated by charging/discharging of pouch cells while applying a preload force. For this purpose, pouch cells were constrained with two different preload force levels of 300 N (12.5 kPa) and 4000 N (167.2 kPa) at 30 % SOC and then charged or discharged to the test SOC, respectively. The pouch cells were tested at 0 %, 30 %, 60 % and 100 % SOC. Mechanical relaxation [49,50] was considered when applying the preload force to create realistic boundary conditions. Tests without preload force were performed at the same SOC as reference. Apart from effects on the indentation force and displacement, the voltage and temperature at different locations were measured allowing for the investigation of the effect of SOC and preload force on the failure behavior. Additionally, post-mortem photos and video during the indentation tests were taken to investigate the failure mechanisms and the dependency of the thermal runaway and failure behavior on the applied boundary condition.

2.1. Specimen

Commercially available NMC622/graphite lithium-ion pouch cells with a nominal capacity of 60 Ah were used within this study, see

Table 1
Basic data of tested specimen.

Parameter	Value
Nominal capacity	60 Ah
Dimension[a]	300 × 110 × 13.36 mm
Cathode/anode material	NMC622/graphite
Max. voltage	4.2 V
Min. voltage	2.5 V
Anode thickness	208 μm
Cathode thickness	172 μm
Separator thickness	15 μm
Layers of cathodes/anodes	31/32

[a] Average thickness at 0 % SOC.

Table 1. The pouch cell had a dimension of 300 × 110 × 13.36 mm. The thickness describes the average thickness of the pouch cell at 0 % SOC. The surface was measured at 175 measurement points distributed over the whole surface [51]. The jellyroll of the pouch cell had a dimension of 260 × 92 mm. More details about the internal structure of the pouch cell can be taken from Appendix A.

2.2. Specimen preparation

The pouch cells were discharged to 0 % SOC with an electric load (Elektro-Automatik EA-EL 9080-340 B). A constant current constant voltage (CC-CV) procedure with a current of 1 C (60 A) and an abort current of 0.1 C were used to discharge to 2.5 V. A relaxation time of 10 min was kept before charging. The pouch cells were charged with a power supply (Elektro-Automatik EA-PSI 9080-340) with 1 C with constant current for 18 min to reach a SOC of 30 %.

2.3. Test setup

A test setup was designed to perform an indentation test without removing the preload force during and after charging/discharging of the pouch cell, see Fig. 1. The test setup consisted of three aluminum plates. The bottom plate (3) was equipped with guiding shafts to guide the middle plate (2) without tilting. The top plate was used to apply the preload force by compressing four parallel-arranged springs. Bolts with fine thread (M16 × 1.25) were screwed into the bottom plate (3) in order to apply the preload force.

Springs representing the stiffness within a battery module were used instead of compression pads. Using springs allowed for more reproducible results and an estimation of the counteracting force of the pouch cell during the indentation. The stiffness of one spring was chosen to achieve an overall stiffness of the test setup of 380 N mm^{-1} representing the stiffness of a typical compression pad used in battery modules. The four springs were selected from a batch considering their length. The stiffness characteristic of the test setup with the four parallel-arranged springs was tested by compression in a hydraulic press. The linearity of the overall system and an overall stiffness of 380 N mm^{-1} was validated by that test. High precision gauge blocks were used to guarantee repeatability for the application of the two different preload force levels.

The middle plate (2) had a hole with a diameter of 41.5 mm and 50 mm and an attached flange to fit the indenter (4). The indenter (4) was made of steel (42CrMo4) and supported itself on the middle plate (2) by the smaller hole. This ensured a constant preload force on the whole surface of the pouch cell. The indenter (4) was guided by a high strength copper alloy bearing with graphite inlets as solid lubricant (MiSUMi MPBZU 40–50).

2.4. Experimental procedure

A preload force F_{pre} of 300 or 4000 N was applied at 30 % SOC in order to represent the mechanical preload force during the battery module manufacturing process [26], respectively. A preload force is commonly applied to the battery cell stack and the battery module's endplates during the manufacturing process. The battery module is then joined while maintaining the preload force [26]. The preload force was readjusted after 10 min to account for mechanical relaxation. Mechanical relaxation caused an asymptotic decrease of the preload force. A

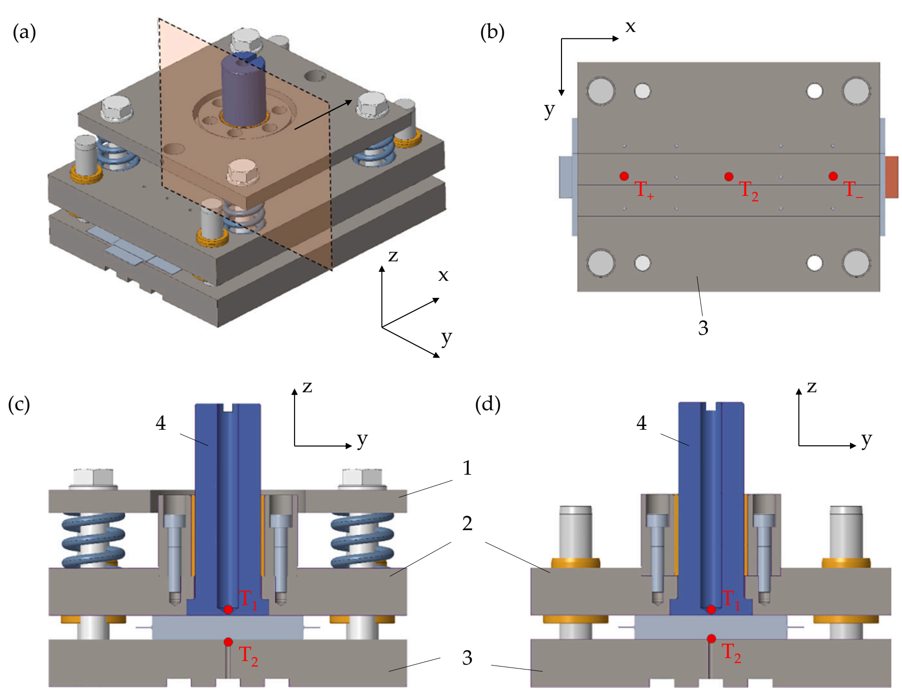

Fig. 1. (a) Test setup for quasi-static indentation tests with cross section plane. (b) Bottom view with bottom plate (3) and three temperature measurement points T_2 in the center and T_+, T_- close the positive and negative battery tabs. (c) Cross section of the test setup for mechanically preloaded tests with top plate (1), guided middle plate (2), bottom plate (3), guided indenter (4) with temperature sensor T_1 and springs. (d) Cross section of the test setup for reference tests without preload force.

period of 10 min was sufficient to reach a mechanical relaxed state of the pouch cell. This was proven by measuring the transient preload force in preliminary investigations by setting the two preload force levels and readjusting it after a period of 10 min.

The test SOC was achieved by discharging the constrained pouch cell with a CC-CV procedure including a current of 1 C and an abort current of 0.1 C to 2.5 V. A relaxation time of 10 min was considered before charging. The pouch cells were then charged with 1 C with constant current for the corresponding time to achieve the test SOC. The distance between the middle (2) and top plate (1) was measured before the indentation tests at two opposite positions to obtain the actual preload force before the quasi-static mechanical test, see Fig. B.2 in Appendix B.

The reference tests without preload force followed the same charging and discharging scheme. In these tests, the test setup was used without springs. Three repetitions were performed for each preload force level F_{pre} (0 N, 300 N and 4000 N) and SOC (0 %, 30 %, 60 % and 100 % SOC), see Table 2.

2.5. Quasi-static indentation test

After constraining the pouch cell and reaching the test SOC, quasi-static indentation tests were performed. The pouch cell's voltage, temperature at various locations, indentation depth and force were measured during the quasi-static indentation tests. The temperature was measured with Type K thermocouples with an accuracy of ± 0.75 °C at four different locations: one thermocouple inside the indenter (4) and three thermocouples distributed over the bottom of the pouch cell, see Fig. 1. The thermocouple inside the indenter (4) was fixed in the indenter's bore hole that was filled with thermal paste to guarantee good thermal conductivity. The three thermocouples on the bottom plate (3) were fixed with adhesive tape and touched the surface of the pouch cell.

The prepared test setup with the pouch cells was placed inside a specific hydraulic press allowing for safe testing under laboratory conditions. The distance between the indenter (4) and the hydraulic press was measured before each test to determine the point of contact. A load cell (HBM Type C6A 500 kN) of the accuracy class 0.5 measured the indentation force. The indenter (4) indented the pouch cell with a speed of 0.2 mm s^{-1} to achieve quasi-static conditions. The indentation was measured with a high-precision linear glass scale encoder (SINO KA-300) with an accuracy of 1 μm. Video was recorded during the indentation to investigate the thermal reaction of the pouch cell at the point of failure. After the indentation test, all parts of the test setup were cleaned. All sliding bearings were lubricated after cleaning to have optimal gliding conditions.

3. Results

3.1. Mechanical behavior

The force-displacement and voltage-displacement curves of the quasi-static mechanical tests for different SOC and different preload force levels can be taken from Fig. 2. The maximum force is in the range of 137 kN to 170 kN and occurs at an indentation between 2.6 mm and 3.8 mm. The force curves indicate a similar shape for 0 %, 30 % and 60 % SOC. The shape changes qualitatively for a SOC of 100 %.

The qualitative change in the force-displacement curves at 100 % SOC indicates a more abrupt mechanical failure of the pouch cells. The mechanical failure of the pouch cells can be characterized by an abrupt drop in force after reaching a maximum force F_{max}. The mechanical failure is not displacement controlled as the hydraulic press cannot regulate the hydraulic pressure in such a short time frame and the force-displacement curves in Fig. 2 can only be interpreted to the point of mechanical failure. A mechanical softening of the pouch cells occurs before the abrupt drop of force for 0 %, 30 % and 60 % SOC, see Fig. C.1 in Appendix C.

In the case of 100 % SOC, a mechanical softening is not observed and the abrupt drop in force coincides with the force maximum F_{max}. This more abrupt mechanical failure results in a peaked shape of the force-displacement curves for 100 % SOC. The preload force was only increasing slightly for 60 % and 100 % SOC due to the SOC-dependent thickness increase caused by reversible swelling, see Table B.2 in Appendix B. The relatively low spring stiffness causes a minor increase of preload force for the additional spring compression by reversible swelling of the pouch cells. The minor change in preload force by SOC-dependent thickness increase can explain that the abrupt drop in force can be observed for all levels of preload force for 100 % SOC.

The more abrupt failure of the pouch cells at 100 % SOC can be the result of an earlier failure of fully lithiated graphite anodes under tensile loading [48] and chemical reactions that occur even before mechanical failure. A slight decrease in voltage before mechanical failure indicates an internal short circuit (ISC) with a high short circuit resistance. This implies that a separator damage is already initiated before the mechanical failure. The separator damage is more severe with a 100 % SOC pouch cell potentially causing the qualitative change in the mechanical behavior and affecting the test repeatability especially for the 100 % SOC tests.

In general, a preload force reduces the spread between the tests. The application of a preload force causes more reproducible initial conditions before the quasi-static indentation test by flattening the unevenness and irregular thickness of the pouch cell surface.

3.1.1. Maximum indentation force

The maximum indentation force F_{max} shows only minor dependence on the SOC, see Fig. 3(a). The tests without preload force have a wide spread between 143 kN and 170 kN averaging over all tests at 159 kN. The maximum force F_{max} indicates a dependence on the preload force taking the averaged values into consideration. The pouch cells without preload force are sustaining the highest force on average before mechanical failure except from 100 % SOC. The maximum force for a preload force of 300 N and 4000 N is ranging from 148 kN to 159 kN (average 153 kN) and from 137 kN to 162 kN (average 153 kN), respectively. The maximum force F_{max} at both levels of preload force are on average close to each other but are significantly smaller than the maximum force measured during experiments without preload force, see Table 3.

Several influencing factors are attributed to the preload force dependency of the maximum indentation force F_{max}. Internal stress caused by the preload force reduces the additional mechanical load that can be sustained by the pouch cells. This might lead to a higher maximum indentation force for pouch cells that are not mechanically preloaded. Additionally, a free deformation of the pouch cell is restricted by the mechanical constraint causing altered deformation patterns. A mechanically constrained pouch cell is not able to bend up (lifting of the edges) during indentation to the same extent as a mechanically unconstrained pouch cell. The lifting edges of the mechanically unconstrained pouch cell cause the middle plate of the test setup to move upwards during indentation.

3.1.2. Displacement at maximum indentation force

The displacement d_{Fmax} indicates the indenter displacement with the maximum indentation force F_{max}. On average, pouch cells without preload force show a larger indenter displacement at maximum force d_{Fmax} except for 30 % SOC, see Fig. 3(b). The displacement d_{Fmax} varies from 2.85 mm to 3.79 mm for a pouch cell without preload force. The

Table 2
Test matrix with the performed tests.

F_{pre} [N]	SOC [%]	No. of repetitions
0 300 4000	0, 30 60, 100	3

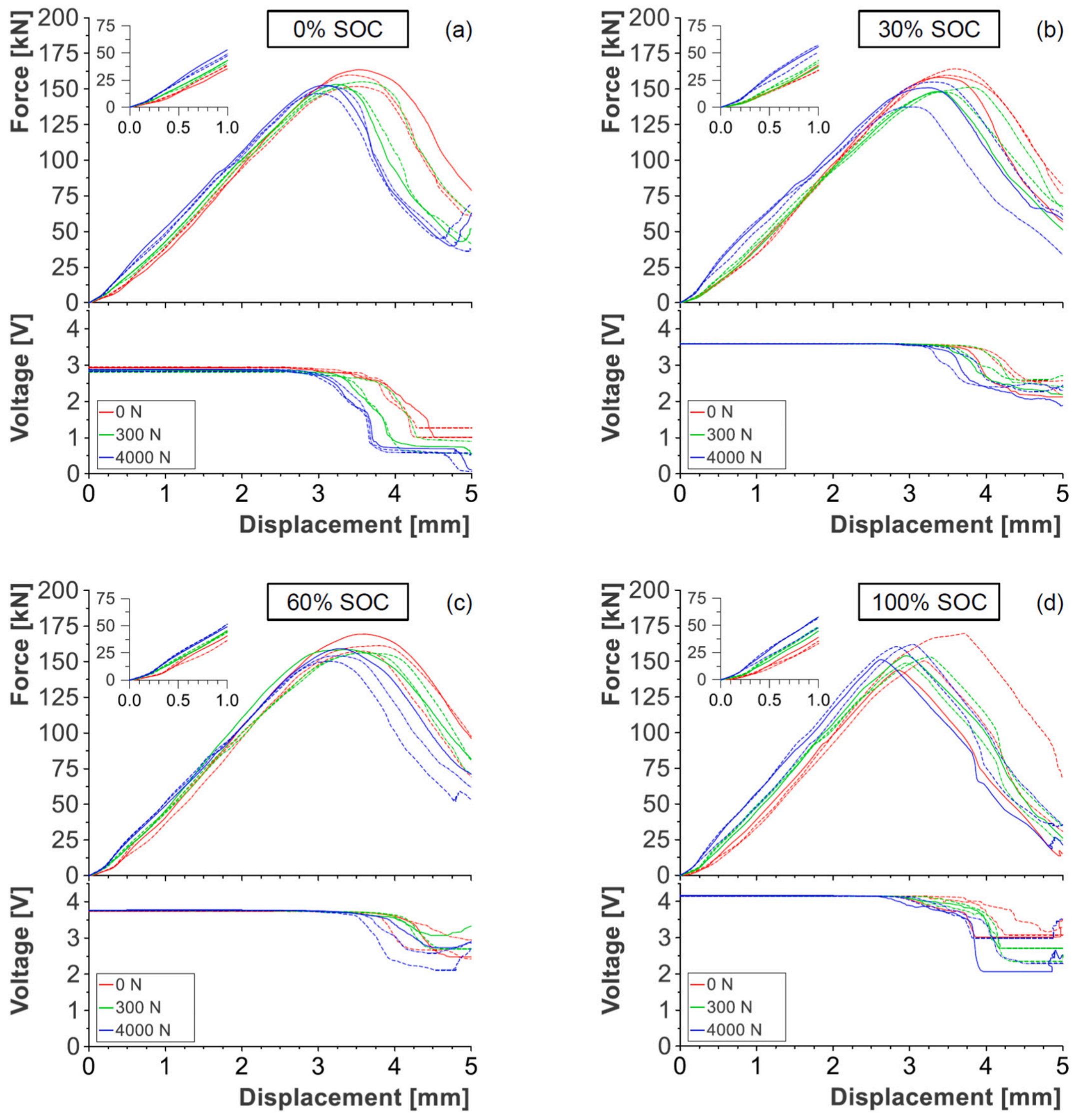

Fig. 2. Results of quasi-static indentation tests for different levels of preload force and SOC. (a) 0 % SOC. (b) 30 % SOC. (c) 60 % SOC. (d) 100 % SOC.

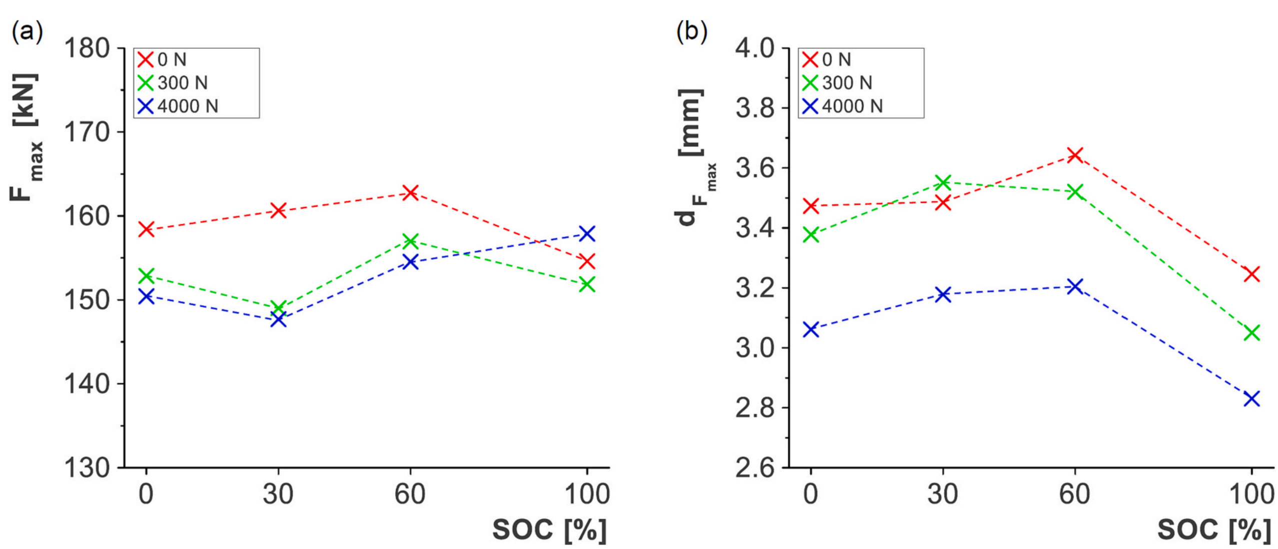

Fig. 3. Arithmetic mean of experimental results for (a) maximum force F_{max} and (b) corresponding displacement of the indenter d_{Fmax}.

displacement d_{Fmax} for a pouch cell with a preload force of 300 N is close to the one without preload force ranging from 2.95 mm to 3.82 mm. At a preload force of 4000 N, the displacement d_{Fmax} ranging from 2.62 mm to 3.32 mm is on average (3.07 mm) significantly lower compared to the other two levels of preload force (3.46 mm for 0 N and 3.38 mm for 300 N).

Increasing the preload force on the pouch cells causes a maximum force F_{max} at a lower indenter displacement d_{Fmax}. The preload force causes a pre-compression and compaction of the internal structure of the pouch cell. The porosity of the electrodes and separator are reduced by the applied preload force decreasing the amount of mechanically sustainable deformation. A preload force of 300 N or 4000 N caused on average a reduction of the pouch cell's thickness of 0.07 mm and 0.27 mm, respectively.

Additionally, the unevenness of the surface of the pouch cells is flattened by a preload force. The initial indentation phase of an unconstrained pouch cell consists of the flattening of the indented surface by the indenter. The initial flattening of the indented surface causes only a minor mechanical load to the internal structure resulting in a larger tolerable indentation for unconstrained pouch cells.

3.1.3. Mechanical stiffness

The force-displacement curves have two nearly linear sections before the maximum force F_{max}, see Fig. 2. The two stiffness values c_1 and c_2 were calculated with a linear regression of the force-displacement curve considering the displacement ranging from 0 mm to 0.2 mm and 0.5 mm to 1.5 mm, respectively. Fig. 4(a) and (b) illustrates the two obtained stiffness values c_1 and c_2. Average values for the stiffness can be taken from Table 3. Both stiffness values show no clear dependency on SOC.

The stiffness c_1 indicates a dependency on the preload force of the pouch cell. Except from 30 % SOC, pouch cells without preload force have the lowest stiffness c_1 ranging from 9.7 kN mm^{-1} to 21.3 kN mm^{-1} (average 17.4 kN mm^{-1}). Increasing the preload force leads to a stiffening of pouch cells at low displacement. This can be attributed to the internal stress by pre-compression and a flattening of the surface of the pouch cell. The stiffness c_1 increases for a preload force of 300 N ranging from 14.6 kN mm^{-1} to 29.9 kN mm^{-1} (average 23.2 kN mm^{-1}). A further increase of the preload force to 4000 N leads to a further increase of the stiffness c_1 ranging from 28.5 kN mm^{-1} to 40.1 kN mm^{-1} (average 33.5 kN mm^{-1}). A mechanically unconstrained pouch cell is softer at the beginning of indentation.

The stiffness c_1 approaches the value of the stiffness c_2 when increasing the preload force indicating a material compaction and flattening of the unevenness of the pouch cell. This is also indicated by the independence of the stiffness c_2 on the preload force, see Fig. 4(b). The stiffness c_2 ranges from 49.3 kN mm^{-1} to 61.2 kN mm^{-1} (average 53.6 kN mm^{-1}) for all indentation tests. This was expected as the applied preload force is rather low compared to the indentation force.

3.2. Failure behavior

The measured voltage, temperature and video are investigated in order to find out the influence of the mechanical preload and the SOC on the failure behavior of the pouch cells. The indenter applies a mechanical load to the pouch cell until a mechanical failure occurs. A pouch cell without preload force bends up and lifts the middle plate of the test setup during indentation, see Fig. 5(a). The deformation of a constrained pouch cell with preload force is blocked and the pouch cell is not able to bend up, see Fig. 5(d)–(e).

The shape of the indenter is punched into the pouch cell leading to a rupture of the separator at the indenter edge resulting in an external short circuit, see Fig. 5(b). In the case of high SOC the produced short circuit leads to a thermal runaway of the pouch cell. Internal pressure and temperature rise by chemical reactions until the flammable gas ignites, see Fig. C.1. The internal pressure in the pouch cell during thermal runaway is strong enough to lift the top plate against the preload force and the additional counter force applied through the springs, see Fig. 5(d)–(e). The burning gas leaves the pouch cell on the long side of the pouch seam and opens the whole side. Increasing the preload force results in a more directed and higher pressurized outgassing of the thermal runaway gasses indicated by the traces of smoke and particles from the combustion after the experiment, see Fig. 5(c)–(e). A pouch cell without preload force indicates thermal runaway marks over the entire cell body. Pouch cells with a preload force show a less affected overall area due to the directed and pressurized outgassing.

3.2.1. Short circuit

The pouch cell's voltage can be characterized by a slight decrease followed by a sharp voltage drop, see Fig. 2. The displacement d_{Vdrop} of the indenter at a voltage drop of 0.05 V can be taken from Fig. 6(a) and was defined as the short circuit point according to the literature [12]. A dependency of d_{Vdrop} on the SOC is found. The earliest voltage drop occurs on average at 0 % SOC and shifts towards a higher displacement for 30 % SOC and 60 % SOC. At 100 % SOC the displacement at voltage drop d_{Vdrop} decreases. A comparison of the displacement at the voltage drop d_{Vdrop} with the displacement at the maximum force d_{Fmax} is given in Table 3. The comparison reveals that at 30 % SOC, 60 % SOC and 100 % SOC a voltage drop occurs after or very close to the maximum force. At 0 % SOC, the voltage drop occurs significantly earlier than the maximum force.

The slight decrease in voltage indicates a short circuit with a large ISC resistance as shown for instance by Liu et al. [52]. Further indentation of the pouch cell decreases the ISC resistance and causes a sharp voltage drop that coincides with the mechanical failure, see Fig. C.1 in Appendix C.

The voltage drop at a specific SOC shows a dependency on the preload force. The earliest voltage drop is observed for a preload force of 4000 N ranging from 2.64 mm to 3.31 mm (average 2.99 mm). The displacement for the voltage drop is higher at a preload force of 300 N (average 3.20 mm) and 0 N (average 3.32 mm) ranging from 2.81 mm to 3.67 mm and 2.78 mm to 3.77 mm, respectively. The difference in the voltage drop displacement d_{Vdrop} between 300 N and 0 N is significantly smaller than the difference between 300 N and 4000 N. This effect is expected and is attributed to the internal stress in the separator and the pre-compression of the pouch cell by high mechanical preload. The pre-compression of the pouch cell leads to higher mechanical loads for a smaller displacement.

3.2.2. Maximum temperature

The temperature increases in all experiments directly after the mechanical failure triggered by the external short circuit. A higher SOC leads to higher peak temperatures as expected, see Fig. C.1 in Appendix C. The preload force seems to have an effect on the peak temperatures of the temperature sensor T_1 placed inside the indenter. The other temperature sensors were not used for this evaluation as some sensors have been broken during the indentation test as a result of high temperatures. An investigation of the results reveals on average higher temperature peaks of T_1 for a pouch cell without preload force, see Fig. 6(b). For a preload force of 4000 N on average a lower maximum temperature is observed but still with a significantly higher value than experiments performed under a preload force of 300 N.

3.3. Summary

Table 3 summarizes the average values of the investigated parameters. The values noted in brackets describe the percentage change of a constrained pouch cell in comparison to the unconstrained pouch cells used as reference tests.

Table 3
Average values of different evaluation parameters and percentage difference compared to a pouch cell without preload force $F_{pre} = 0$ N in brackets.

Parameter	$F_{pre} = 0$ N	$F_{pre} = 300$ N	$F_{pre} = 4000$ N	SOC [%]
c_1 [kN mm^{-1}]	20.6	27.5 (+33.6 %)	32.4 (+57.1 %)	0
	19.4	18.0 (−7.3 %)	35.4 (+82.2 %)	30
	17.0	26.8 (+57.8 %)	29.5 (+73.8 %)	60
	12.7	20.6 (+62.5 %)	36.7 (+189.2 %)	100
c_2 [kN mm^{-1}]	51.6	52.7 (+2.2 %)	53.6 (+4.0 %)	0
	50.6	52.1 (+3.0 %)	51.6 (+2.0 %)	30
	54.0	55.1 (+1.9 %)	53.0 (−1.9 %)	60
	53.5	56.3 (+5.3 %)	58.7 (+9.7 %)	100
F_{max} [kN]	158	153 (−3.5 %)	150 (−5.0 %)	0
	161	149 (−7.2 %)	148 (−8.1 %)	30
	163	157 (−3.6 %)	155 (−5.0 %)	60
	155	152 (−1.8 %)	158 (+2.1 %)	100
d_{Fmax} [mm]	3.47	3.38 (−2.7 %)	3.06 (−11.9 %)	0
	3.49	3.55 (+1.9 %)	3.18 (−8.8 %)	30
	3.64	3.52 (−3.4 %)	3.21 (−12.0 %)	60
	3.25	3.05 (−6.0 %)	2.83 (−12.8 %)	100
d_{Vdrop} [mm]	2.93	2.90 (−1.1 %)	2.75 (−6.0 %)	0
	3.49	3.37 (−3.3 %)	3.10 (−11.0 %)	30
	3.56	3.46 (−2.8 %)	3.22 (−9.8 %)	60
	3.28	3.08 (−6.3 %)	2.87 (−12.4 %)	100

3.4. Limitations

The indenter represents an area load on the pouch cell. In crash scenarios other shapes may intrude and indent the battery cell. These types of indenters should be accounted for in the future and the effect of preload force, SOC and reversible swelling should be elaborated.

The tests were performed under quasi-static conditions and should be carried out at crash-relevant loading speeds in future to include strain rate effects such as stiffening of material and qualitative change in failure behavior [16,53,54].

Additionally, the test setup stiffness should be varied and adapted to a non-linear behavior representing the stiffness of a battery module. Components within the battery module such as cooling plates additionally influence the overall stiffness [15]. In the literature, a correlation between reversible swelling and the stiffness against which the battery cell has to expand was found [18]. The stiffness thus has a direct impact on the internal stresses of the battery cell affecting its failure behavior.

4. Conclusions

In this study, the influence of preload force and SOC on the mechanical behavior and failure behavior during mechanical abuse testing of constrained and unconstrained pouch cells was investigated. A suitable test setup was presented to perform out-of-plane indentation tests with realistic boundary conditions. The pouch cells were constrained with a preload force of 300 N or 4000 N at 30 % SOC before indentation. The test SOCs of 0 %, 30 %, 60 % and 100 % were set without removing the preload force of the pouch cell to account for mechanical relaxation. The mechanical abuse load was applied with a flat-end cylinder in the thickness direction of the pouch cell. In order to achieve realistic boundary conditions the preload force was applied via springs representing the stiffness of a commercial compression pad. Reference tests were performed without applying a preload force to the pouch cell.

The mechanical properties were analyzed in terms of maximum indentation force F_{max} and two stiffness values c_1 and c_2. The stiffness c_1 was evaluated at a small indentation below 0.2 mm. The stiffness c_2

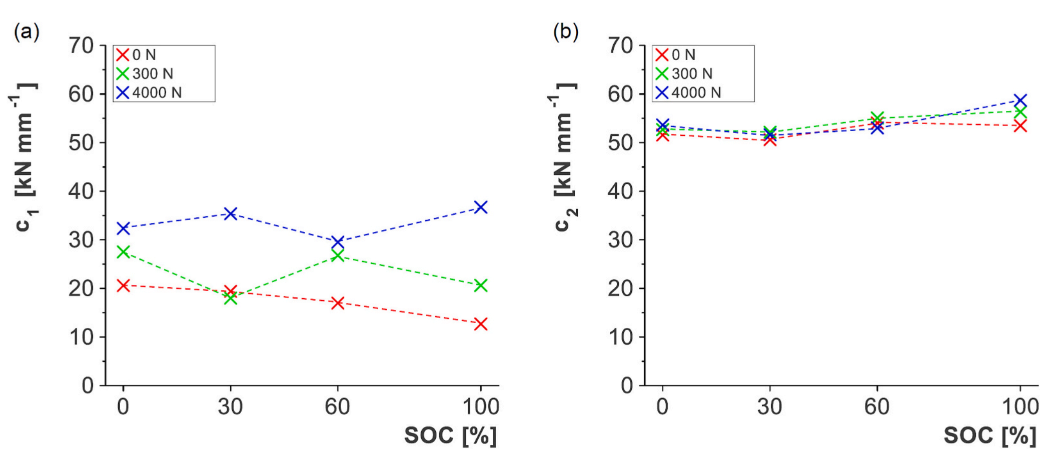

Fig. 4. Arithmetic mean of experimental results for stiffness (a) c_1 evaluated for a displacement of 0 mm to 0.2 mm and (b) c_2 evaluated for a displacement of 0.5 mm to 1.5 mm.

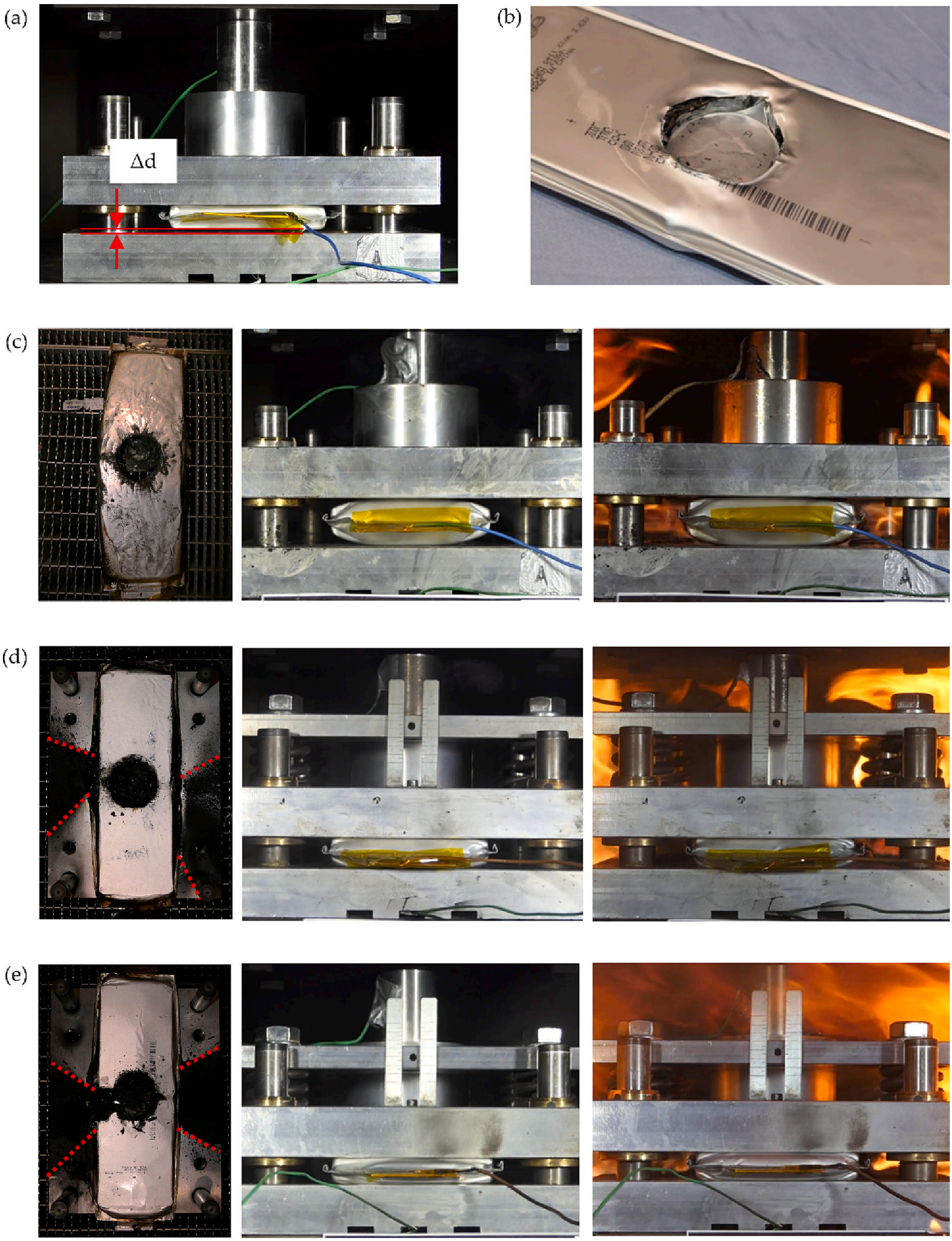

Fig. 5. (a) Lifting of middle plate Δd for a pouch cell without preload force. Post-mortem photo documentation indicating particle traces from combustion (red dashed line) and video sequence right before and during thermal runaway of a pouch cell with (b) 0 % SOC and 0 N preload force, (c) 60 % SOC and 0 N preload force, (d) 60 % SOC and 300 N preload force and (e) 60 % SOC and 4000 N preload force. (For interpretation of the references to color in this figure legend, the reader is referred to the web version of this article.)

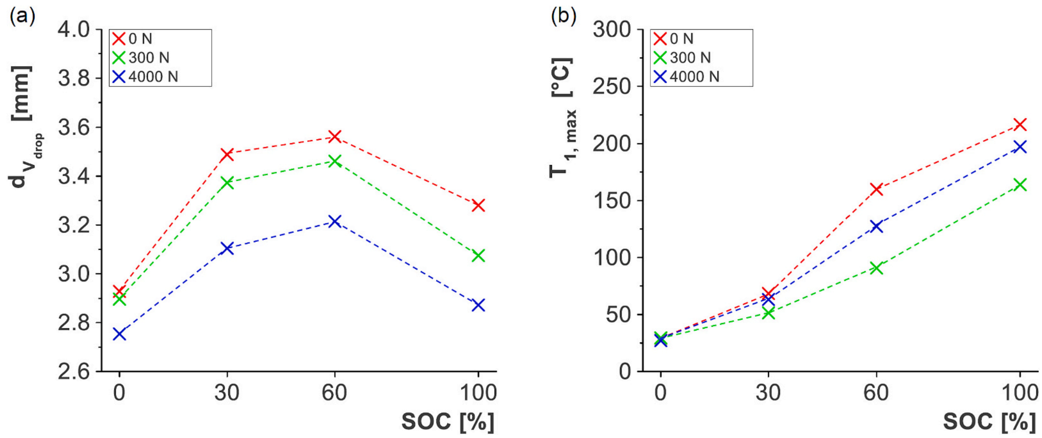

Fig. 6. Arithmetic mean of experimental results for (a) indenter displacement d_{Vdrop} at voltage drop of 0.05 V and (b) maximum temperature of temperature sensor T_1 inside of the indenter.

represented a larger indentation and was evaluated for an indentation between 0.5 mm and 1.5 mm.

The maximum force F_{max} indicated a negative dependency on the preload force explained by initial stress within the jellyroll. The maximum indentation force F_{max} a pouch cell was able to sustain reduced on average by 4.0 % and 4.1 % for a preload force of 300 N or 4000 N. A minor overestimation of the maximum force F_{max} is expected if abuse tests were performed without preload force with a similar indenter geometry.

The stiffness c_1 at small indentations indicated on average a strong positive dependence on preload force resulting from pre-compression of the pouch cell. The stiffness c_1 increased on average by 33.3 % and 92.3 % for a preload force of 300 N or 4000 N. Considering a battery module with several stacked pouch cells, these results indicate a high relevance for numerical simulation models and battery module designing. The stiffness c_1 approaches the stiffness c_2 for a preload force of 4000 N as expected. The stiffness c_2 showed only minor dependency on the variation parameters SOC and preload force and increased on average by 3.2 % and 3.6 % for a preload force of 300 N or 4000 N. The stiffness c_2 for a large indentation is only slightly underestimated when tests are performed without preload force on simplified test setups and with a similar indenter geometry.

In the case of failure behavior, the boundary conditions must be considered. The compression of a pouch cell by preload force shifts the force-displacement curve to the left and imposes mechanical stress in the separator leading to an earlier mechanical and electrical failure indicated by the indentation at the maximum force d_{Fmax} and the voltage drop d_{Vdrop}. The voltage drop occurred significantly earlier than the maximum force when performing the indentation test with 0 % SOC. At other SOC levels both failure mechanisms coincided.

In terms of indentation, the voltage drop d_{Vdrop} occurred on average 3.4 % and 9.9 % earlier for a preload force of 300 N or 4000 N. The indentation causing a voltage drop is of high interest for safety evaluations and is underestimated in the presented work when no preload force is applied.

The conclusions drawn from the presented study are summarized in the following:

- Mechanical characterization for large indentation might be performed without preload force on simplified test setups when the failure behavior is not of interest as the stiffness c_2 correlated with large indentation between 0.5 mm and 1.5 mm is not relevantly dependent on SOC or preload force.
- The stiffness c_1 for a small indentation below 0.2 mm is strongly dependent on preload force and increased with the applied preload force. Performing a mechanical characterization without boundary conditions can lead to a misinterpretation on battery module level, since the error of several battery cells in a battery module is accumulated.
- Internal stress caused by a preload force and reversible swelling affects the failure behavior of pouch cells indicated by a preload force dependency of the maximum force F_{max}, corresponding indentation d_{Fmax} and indentation at voltage drop d_{Vdrop}.
- Application of realistic boundary conditions results in a different failure behavior of pouch cells in quasi-static out-of-plane indentation tests by earlier failure and thermal runaway with high internal pressure leading to a directed out-gassing.

The test results from this study indicate the need for a correct representation of boundary conditions during abuse testing. Important safety relevant load limits were overestimated in this study when no boundary conditions were applied to the pouch cells. Normally, abuse tests with battery cells are performed without consideration of boundary conditions that are imposed by the battery module. This might lead to the derivation of incorrect safety relevant load limits and failure mechanisms. Further investigations can contribute to a deeper understanding of the influence of the applied boundary conditions on the overall mechanical and failure behavior of battery cells in battery modules.

CRediT authorship contribution statement

Patrick Höschele: Conceptualization, Methodology, Validation, Investigation, Writing – original draft, Writing – review & editing, Visualization, Funding acquisition. **Simon F. Heindl:** Conceptualization, Methodology, Writing – review & editing, Project administration, Funding acquisition. **Simon Erker:** Writing – review & editing. **Christian Ellersdorfer:** Conceptualization, Methodology, Writing – review & editing, Supervision.

Declaration of competing interest

The authors declare that they have no known competing financial interests or personal relationships that could have appeared to influence the work reported in this paper.

Data availability

Data will be made available on request.

Acknowledgments

The presented work was conducted within the scope of the research project BonuS in cooperation with the Institute for Chemistry and Technology of Materials at Graz University of Technology and AVL List GmbH, Graz. BonuS has received funding from AVL List GmbH, Graz and the Austrian Research Promotion Agency (FFG) (Grant agreement no. 874834).

Appendix A. Specimen dimension and internal structure

The internal structure of the pouch cell consisted of alternating electrode stacks made up of two anode layers and one cathode layer or one anode layer and two cathode layers, respectively. The electrodes within one stack were separated by a separator sheet. One long separator sheet was used to wrap the electrode stacks starting from the center of the pouch cell, see Fig. A.1.

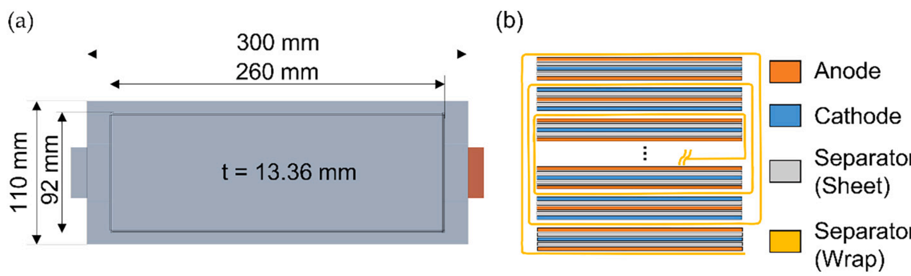

Fig. A.1. (a) Dimensions of tested pouch cell. (b) Schematic sketch of internal cell structure.

Appendix B. Thickness change

The average thickness of unconstrained pouch cells at different SOC was measured with high-precision capacitive sensors (Micro-Epsilon CSE3). The capacitive sensor had an accuracy of ±0.012 μm. The measurement points were distributed over the whole surface of the pouch cell and a total number of 175 measurement points were taken as described by Michelini et al. [51], see Fig. B.1. The average thickness t_{avg} was determined by calculating the arithmetic mean of the 175 measurement points of three pouch cells. The thickness measurements were repeated three times for each pouch cell to validate the results. The average thickness and percentage thickness increase can be taken from Table B.1.

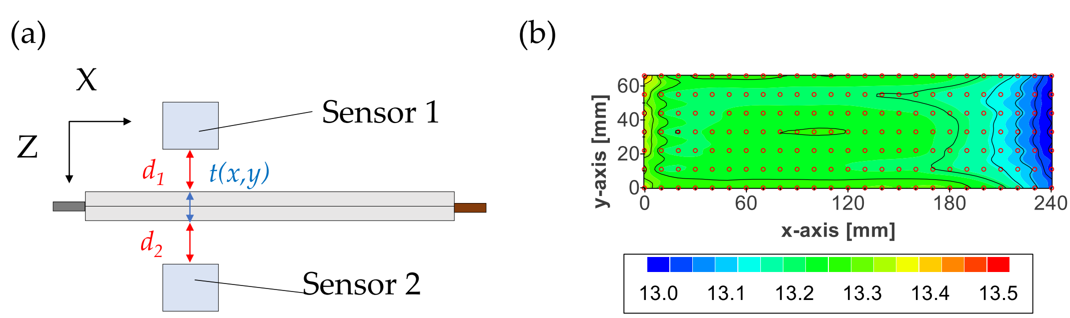

Fig. B.1. (a) Principle sketch of the setup for measuring the thickness of the pouch cell. (b) Exemplary results of the local thickness of the pouch cell with the 175 measurement points indicated by red circles.

Table B.1
Average thickness of an unconstrained pouch cell and the percentage thickness increase compared to 0 % SOC in brackets.

Parameter	SOC = 0 %	SOC = 30 %	SOC = 60 %	SOC = 100 %
t_{avg} [mm]	13.36 (–)	13.54 (1.35 %)	13.60 (1.80 %)	13.75 (2.92 %)

The thickness of the pouch cells reduced on average by 0.07 mm and 0.27 mm when applying a preload force F_{pre} of 300 N or 4000 N, respectively. Additionally, the distance between the middle plate and the top plate was measured at two opposite positions with a vernier height gauge, see Fig. B.2.

The average change of the two measured distances (distance 1 and distance 2) was used to calculate the average change in plate distance Δd_{avg}. Table B.2 summarizes the arithmetic mean of the average change in plate distance Δd_{avg} for all tests performed.

The distance Δd_{avg} was used to calculate the actual compression force that was reached after setting the SOC for indentation testing. The thickness of the pouch cell changed during charging and discharging leading to a change of the initial preload force applied at 30 % SOC, see Table B.2. An increase of the thickness of the pouch cells while charging causes a reduction of the distance Δd_{avg} and results in an increase of the preload force. A decrease of thickness causes an increase of the distance Δd_{avg} and results in a decrease of the preload force.

The change of preload force was small at an initial preload force F_{pre} of 4000 N. For an initial preload force of 300 N a significant change was only observed at 100 % SOC.

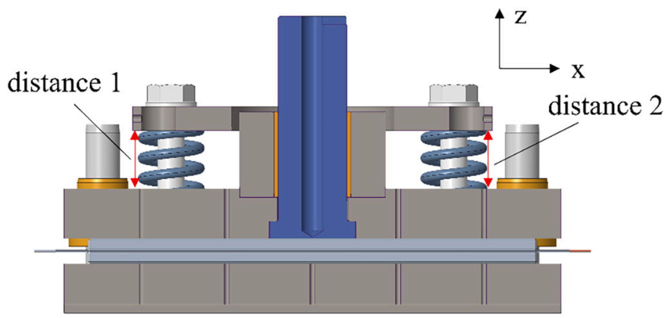

Fig. B.2. Measurement points to set the pretension and derive the force after setting the SOC.

Table B.2
Arithmetic mean of average plate distance Δd_{avg} and resulting change of initial preload force after setting SOC in brackets.

Parameter	$F_{pre} = 300$ N	$F_{pre} = 4000$ N	SOC [%]
Δd_{avg} [mm]	+0.07 (−22.8 N)	+0.22 (−83.6 N)	0
	+0.00 (−0.0 N)	+0.01 (−3.8 N)	30
	−0.02 (+7.6 N)	−0.01 (+3.8 N)	60
	−0.22 (+83.6 N)	−0.17 (64.6 N)	100

Appendix C. Mechanical failure

Fig. C.1 illustrates a time-based representation of the indentation force, indenter displacement, voltage and temperature change for the temperature sensors T_1 and T_2. The mechanical failure occurs at the abrupt drop in force. The mechanical failure occurs shortly after reaching the maximum force for 0 %, 30 % and 60 % SOC. In the case of 100 % SOC the point of mechanical failure nearly coincidences with the point of maximum force. This change in mechanical failure behavior is not dependent on the applied preload force and must therefore be the results of SOC-dependent structural changes within the pouch cell.

The abrupt change of indenter displacement at the point of mechanical failure occurs because the hydraulic press is unable to regulate the hydraulic pressure in such a short time frame.

The obvious drop in voltage coincides with the point of mechanical failure. This result is not obvious in the displacement-based representation illustrated in Fig. 2. The slight decrease in voltage before the obvious voltage drop indicates that an internal short circuit (ISC) is already present before the mechanical failure. A high ISC resistance causes only a slight reduction of voltage. The voltage drops further in the event of an increasing indentation. No permanent short circuit was observed for 30 % SOC and a preload force of 300 N. Similar results were found in a study by Liu et al. [52]. No permanent short circuit was observed in this study for a medium SOC. The authors described that in the medium SOC range current collector melting is dominant in comparison to separator melting.

The temperature sensors T_1 and T_2 indicate a temperature increase coinciding with the point of mechanical failure. The ISC triggers exothermic reactions and results in a thermal runaway for tests performed at 60 % and 100 % SOC. Tests performed at 0 % and 30 % SOC show only a slight temperature increase.

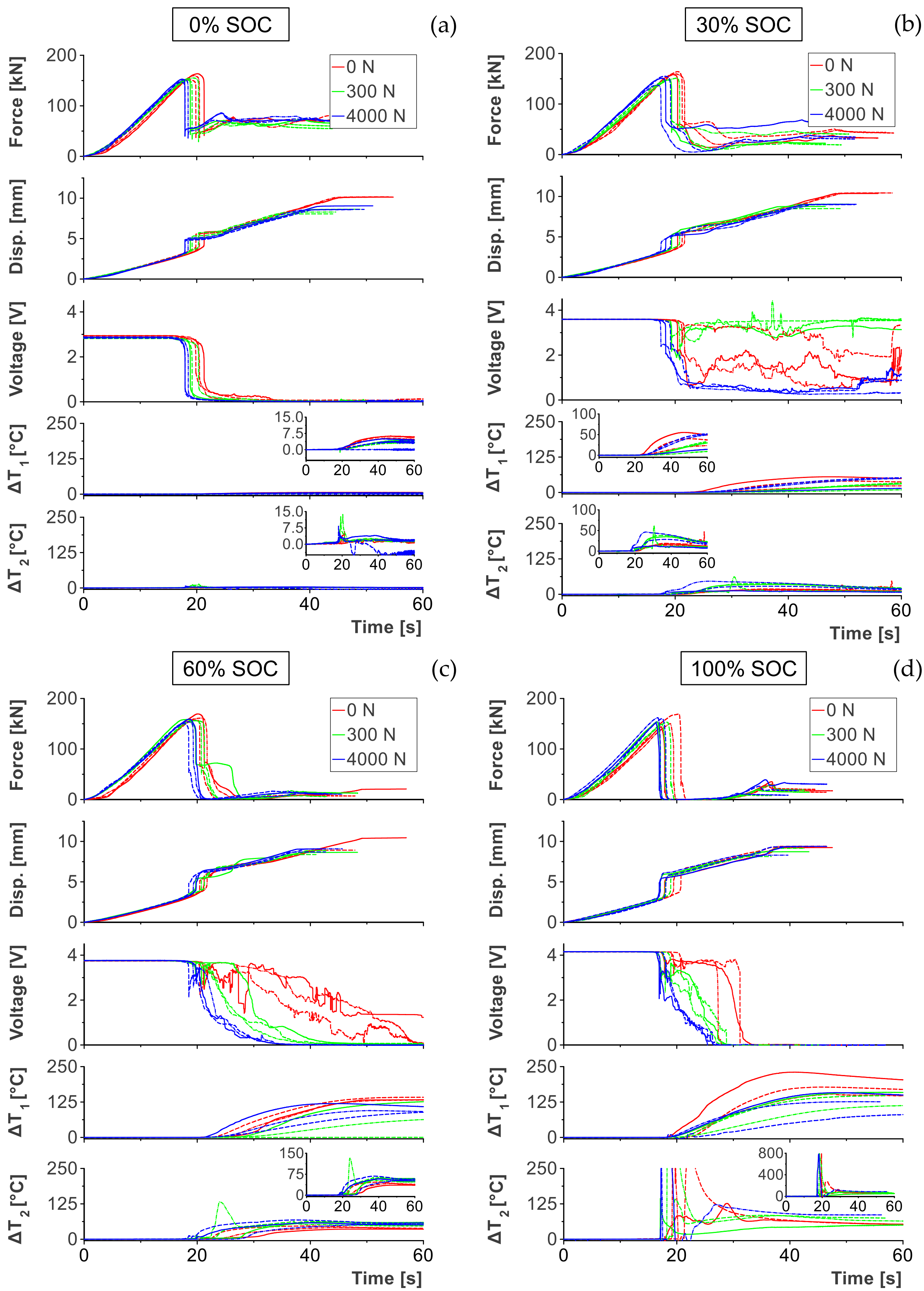

Fig. C.1. Force, displacement, voltage and change of temperature ΔT_1 and ΔT_2 over time for quasi-static mechanical tests for different levels of preload force and SOC. (a) 0 % SOC. (b) 30 % SOC. (c) 60 % SOC. (d) 100 % SOC.

References

[1] X. Zeng, M. Li, D.Abd El-Hady, W. Alshitari, A.S. Al-Bogami, J. Lu, K. Amine, Commercialization of lithium battery technologies for electric vehicles, Adv. Energy Mater. 9 (27) (2019), 1900161, https://doi.org/10.1002/aenm.201900161.

[2] X. Feng, M. Ouyang, X. Liu, L. Lu, Y. Xia, X. He, Thermal runaway mechanism of lithium ion battery for electric vehicles: a review, Energy Storage Mater. 10 (3) (2018) 246–267, https://doi.org/10.1016/j.ensm.2017.05.013.

[3] A.R. Baird, E.J. Archibald, K.C. Marr, O.A. Ezekoye, Explosion hazards from lithium-ion battery vent gas, J. Power Sources 446 (2020), 227257, https://doi.org/10.1016/j.jpowsour.2019.227257.

[4] H. Wang, H. Xu, Z. Zhang, Q. Wang, C. Jin, C. Wu, C. Xu, J. Hao, L. Sun, Z. Du, Y. Li, J. Sun, X. Feng, Fire and explosion characteristics of vent gas from lithium-ion batteries after thermal runaway: a comparative study, eTransportation 13 (2022), 100190, https://doi.org/10.1016/j.etran.2022.100190.

[5] J. Kukreja, T. Nguyen, T. Siegmund, W. Chen, W. Tsutsui, K. Balakrishnan, H. Liao, N. Parab, Crash analysis of a conceptual electric vehicle with a damage tolerant battery pack, Extreme Mech.Lett. 9 (2016) 371–378, https://doi.org/10.1016/j.eml.2016.05.004.

[6] L. Scurtu, I. Szabo, F. Mariasiu, D. Moldovanu, L. Mihali, A. Jurco, Numerical analysis of the influence of mechanical stress on the battery pack's housing of an electric vehicle, IOP Conf.Ser.Mater.Sci.Eng. 568 (2019), 012054, https://doi.org/10.1088/1757-899X/568/1/012054.

[7] J. Zhu, T. Wierzbicki, W. Li, A review of safety-focused mechanical modeling of commercial lithium-ion batteries, J. Power Sources 378 (2018) 153–168, https://doi.org/10.1016/j.jpowsour.2017.12.034.

[8] Q. Wang, B. Mao, S.I. Stoliarov, J. Sun, A review of lithium ion battery failure mechanisms and fire prevention strategies, Prog. Energy Combust. Sci. 73 (2019) 95–131, https://doi.org/10.1016/j.pecs.2019.03.002.

[9] L. Aiello, I. Hanzu, G. Gstrein, E. Ewert, C. Ellersdorfer, W. Sinz, Analysis and investigation of thermal runaway propagation for a mechanically constrained lithium-ion pouch cell module, Batteries 7 (3) (2021) 49, https://doi.org/10.3390/batteries7030049.

[10] V. Ruiz, A. Pfrang, A. Kriston, N. Omar, P. van den Bossche, L. Boon-Brett, A review of international abuse testing standards and regulations for lithium ion batteries in electric and hybrid electric vehicles, Renew. Sust. Energ. Rev. 81 (Part1) (2018) 1427–1452, https://doi.org/10.1016/j.rser.2017.05.195.

[11] J. Duan, X. Tang, H. Dai, Y. Yang, W. Wu, X. Wei, Y. Huang, Building safe lithium-ion batteries for electric vehicles: a review, Electrochem.Energy Rev. 3 (2020) 1–42, https://doi.org/10.1007/s41918-019-00060-4.

[12] B. Liu, Y. Jia, C. Yuan, L. Wang, X. Gao, S. Yin, J. Xu, Safety issues and mechanisms of lithium-ion battery cell upon mechanical abusive loading: a review, Energy Storage Mater. 24 (2020) 85–112, https://doi.org/10.1016/j.ensm.2019.06.036.

[13] G. Kermani, E. Sahraei, Review: characterization and modeling of the mechanical properties of lithium-ion batteries, Energies 10 (11) (2017) 1730, https://doi.org/10.3390/en10111730.

[14] Y. Xia, G. Chen, Q. Zhou, X. Shi, F. Shi, Failure behaviours of 100% SOC lithium-ion battery modules under different impact loading conditions, Eng. Fail. Anal. 82 (2) (2017) 149–160, https://doi.org/10.1016/j.engfailanal.2017.09.003.

[15] S. Kalnaus, H. Wang, T.R. Watkins, A. Kumar, S. Simunovic, J.A. Turner, P. Gorney, Effect of packaging and cooling plates on mechanical response and failure characteristics of automotive Li-ion battery modules, J. Power Sources 403 (2–3) (2018) 20–26, https://doi.org/10.1016/j.jpowsour.2018.09.071.

[16] S. Kalnaus, H. Wang, T.R. Watkins, S. Simunovic, A. Sengupta, Features of mechanical behavior of ev battery modules under high deformation rate, Extreme Mech.Lett. 32 (2–3) (2019), 100550, https://doi.org/10.1016/j.eml.2019.100550.

[17] B. Arief Budiman, S. Rahardian, A. Saputro, A. Hidayat, I. Pulung Nurprasetio, P. Sambegoro, Structural integrity of lithium-ion pouch battery subjected to three-point bending, Eng. Fail. Anal. 138 (3) (2022), 106307, https://doi.org/10.1016/j.engfailanal.2022.106307.

[18] J. Cannarella, C.B. Arnold, Stress evolution and capacity fade in constrained lithium-ion pouch cells, J. Power Sources 245 (2014) 745–751, https://doi.org/10.1016/j.jpowsour.2013.06.165.

[19] V. Müller, R.-G. Scurtu, K. Richter, T. Waldmann, M. Memm, M.A. Danzer, M. Wohlfahrt-Mehrens, Effects of mechanical compression on the aging and the expansion behavior of Si/C-Composite|NMC811 in different lithium-ion battery cell formats, J. Electrochem. Soc. 166 (15) (2019) A3796–A3805, https://doi.org/10.1149/2.1121915jes.

[20] R. Li, W. Li, A. Singh, D. Ren, Z. Hou, M. Ouyang, Effect of external pressure and internal stress on battery performance and lifespan, Energy Storage Mater. 52 (2022) 395–429, https://doi.org/10.1016/j.ensm.2022.07.034.

[21] B. Rieger, S. Schlueter, S.V. Erhard, J. Schmalz, G. Reinhart, A. Jossen, Multi-scale investigation of thickness changes in a commercial pouch type lithium-ion battery, J.Energy Storage 6 (9) (2016) 213–221, https://doi.org/10.1016/j.est.2016.01.006.

[22] B. Rieger, S. Schlueter, S.V. Erhard, A. Jossen, Strain propagation in lithium-ion batteries from the crystal structure to the electrode level, J. Electrochem. Soc. 163 (8) (2016) A1595–A1606, https://doi.org/10.1149/2.0431608jes.

[23] H. Pegel, O. von Kessel, P. Heugel, T. Deich, J. Tübke, K.P. Birke, D.U. Sauer, Volume and thickness change of NMC811|SiOx–graphite large-format lithium-ion cells: from pouch cell to active material level, J. Power Sources 537 (23) (2022), 231443, https://doi.org/10.1016/j.jpowsour.2022.231443.

[24] A.J. Louli, J. Li, S. Trussler, C.R. Fell, J.R. Dahn, Volume, pressure and thickness evolution of Li-ion pouch cells with silicon-composite negative electrodes, J. Electrochem. Soc. 164 (12) (2017) A2689–A2696, https://doi.org/10.1149/2.1691712jes.

[25] A.J. Louli, L.D. Ellis, J.R. Dahn, Operando pressure measurements reveal solid electrolyte interphase growth to rank Li-ion cell performance, Joule 3 (3) (2019) 745–761, https://doi.org/10.1016/j.joule.2018.12.009.

[26] T. Deich, S.L. Hahn, S. Both, K.P. Birke, A. Bund, Validation of an actively-controlled pneumatic press to simulate automotive module stiffness for mechanically representative lithium-ion cell aging, J.Energy Storage 28 (2020), 101192, https://doi.org/10.1016/j.est.2020.101192.

[27] M. Wünsch, J. Kaufman, D.U. Sauer, Investigation of the influence of different bracing of automotive pouch cells on cyclic liefetime and impedance spectra, J. Energy Storage 21 (2019) 149–155, https://doi.org/10.1016/j.est.2018.11.019.

[28] Y.H. Choi, H.K. Lim, J.-H. Seo, W.J. Shin, J.H. Choi, J.H. Park, Development of standardized battery pack for next-generation PHEVs in considering the effect of external pressure on lithium-ion pouch cells, SAE Int.J.Altern.Powertrains 7 (3) (2018) 195–205, https://doi.org/10.4271/2018-01-0439.

[29] T. Deich, M. Storch, K. Steiner, A. Bund, Effects of module stiffness and initial compression on lithium-ion cell aging, J. Power Sources 506 (2021), 230163, https://doi.org/10.1016/j.jpowsour.2021.230163.

[30] S. Hahn, S. Theil, J. Kroggel, K.P. Birke, Pressure prediction modelling and validation for lithium-ion pouch cells in buffered module assemblies, J.Energy Storage 40 (2021), 102517, https://doi.org/10.1016/j.est.2021.102517.

[31] A. Li, A.C.Y. Yuen, W. Wang, I.M. de Cachinho Cordeiro, C. Wang, T.B.Y. Chen, J. Zhang, Q.N. Chan, G.H. Yeoh, A review on lithium-ion battery separators towards enhanced safety performances and modelling approaches, Molecules 26 (2) (2021), https://doi.org/10.3390/molecules26020478.

[32] J. Xu, L. Zhu, L. Xiao, H. Hu, Z. Yin, R. Zhang, J.C.-Y. Jung, Z.-G. Shen, P.-C. Sui, A multiscale study on the effect of compression on lithium-ion battery separators, J.Energy Storage 54 (2022), 105255, https://doi.org/10.1016/j.est.2022.105255.

[33] W. Li, Y. Xia, J. Zhu, H. Luo, State-of-charge dependence of mechanical response of lithium-ion batteries: a result of internal stress, J. Electrochem. Soc. 165 (7) (2018) A1537–A1546, https://doi.org/10.1149/2.0051809jes.

[34] E. Sahraei, R. Hill, T. Wierzbicki, Calibration and finite element simulation of pouch lithium-ion batteries for mechanical integrity, J. Power Sources 201 (2012) 307–321, https://doi.org/10.1016/j.jpowsour.2011.10.094.

[35] W.-J. Lai, M.Y. Ali, J. Pan, Mechanical behavior of representative volume elements of lithium-ion battery modules under various loading conditions, J. Power Sources 248 (2014) 789–808, https://doi.org/10.1016/j.jpowsour.2013.09.128.

[36] J. Zhu, M.M. Koch, J. Lian, W. Li, T. Wierzbicki, Mechanical deformation of lithium-ion pouch cells under in-plane loads–part I: experimental investigation, J. Electrochem. Soc. 167 (9) (2020), 090533, https://doi.org/10.1149/1945-7111/ab8e83.

[37] H. Wang, X. Duan, B. Liu, The anisotropic homogenized model for pouch type lithium-ion battery under various abuse loadings, J.Electrochem.Energy Convers. Storage 18 (2) (2021) 95, https://doi.org/10.1115/1.4049239.

[38] B. Xing, F. Xiao, Y. Korogi, T. Ishimaru, Y. Xia, Direction-dependent mechanical-electrical-thermal responses of large-format prismatic Li-ion battery under mechanical abuse, J.Energy Storage 43 (4) (2021), 103270, https://doi.org/10.1016/j.est.2021.103270.

[39] W. Wenwei, L. Yiding, L. Cheng, S. Yuefeng, Y. Sheng, State of chargedependent failure prediction model for cylindrical lithium-ion batteries under mechanical abuse, Appl. Energy 251 (2019), 113365, https://doi.org/10.1016/j.apenergy.2019.113365.

[40] J. Xu, B. Liu, X. Wang, D. Hu, Computational model of 18650 lithium ion battery with coupled strain rate and SOC dependencies, Appl. Energy 172 (2016) 180–189, https://doi.org/10.1016/j.apenergy.2016.03.108.

[41] J. Xu, Y. Jia, B. Liu, H. Zhao, H. Yu, J. Li, S. Yin, Coupling effect of state-of-health and state-of-charge on the mechanical integrity of lithium-ion batteries, Exp. Mech. 58 (4) (2018) 633–643, https://doi.org/10.1007/s11340-018-0380-9.

[42] M. Spielbauer, M. Steinhardt, J. Singer, A. Aufschläger, O. Bohlen, A. Jossen, Influence of breathing and swelling on the jelly-roll case gap of cylindrical lithium-ion battery cells, Batteries 9 (1) (2023) 6, https://doi.org/10.3390/batteries9010006.

[43] P. Kotter, T. Kisters, A. Schleicher, Dynamic impact tests to characterize the crashworthiness of large-format lithium-ion cells, J.Energy Storage 26 (8) (2019), 100948, https://doi.org/10.1016/j.est.2019.100948.

[44] T. Wang, X. Chen, G. Chen, H. Ji, L. Li, Q. Yuan, Y. Liu, Y. Ji, Investigation of mechanical integrity of prismatic lithium-ion batteries with various state of charge, J.Electrochem.Energy Convers.Storage 18 (3) (2021) 928, https://doi.org/10.1115/1.4048330.

[45] H. Luo, Y. Xia, Q. Zhou, Mechanical damage in a lithium-ion pouch cell under indentation loads, J. Power Sources 357 (2017) 61–70, https://doi.org/10.1016/j.jpowsour.2017.04.101.

[46] Y. Qu, B. Xing, C. Wang, Y. Xia, Simplified layered model of pouch cell for varied load cases: an indentation and three-point bending study, J.Energy Storage 59 (11) (2023), 106476, https://doi.org/10.1016/j.est.2022.106476.

[47] Y. Qi, L.G. Hector, C. James, K.J. Kim, Lithium concentration dependent elastic properties of battery electrode materials from first principles calculations, J. Electrochem. Soc. 161 (11) (2014) F3010–F3018, https://doi.org/10.1149/2.0031411jes.

[48] Z. Pan, T. Sedlatschek, Y. Xia, Effect of state-of-charge and air exposure on tensile mechanical properties of lithium-ion battery electrodes, J. Electrochem. Soc. 167 (9) (2020), 090517, https://doi.org/10.1149/1945-7111/ab8804.

[49] J.P. Singer, C. Sämann, T. Gössl, K.P. Birke, Pressure monitoring cell for constrained battery electrodes, Sensors 18 (11) (2018), https://doi.org/10.3390/s18113808.

[50] O. von Kessel, T. Deich, S. Hahn, F. Brauchle, D. Vrankovic, T. Soczka-Guth, K. P. Birke, Mechanical impedance as a tool for electromechanical investigation and equivalent modeling of lithium-ion batteries, J. Power Sources 508 (19) (2021), 230337, https://doi.org/10.1016/j.jpowsour.2021.230337.
[51] E. Michelini, P. Höschele, S.F. Heindl, S. Erker, C. Ellersdorfer, Experimental investigation on reversible swelling mechanisms of lithium-ion batteries under a varying preload force, Batteries 9 (4) (2023) 218, https://doi.org/10.3390/batteries9040218.
[52] B. Liu, Y. Jia, J. Li, S. Yin, C. Yuan, Z. Hu, L. Wang, Y. Li, J. Xu, Safety issues caused by internal short circuits in lithium-ion batteries, J. Mater. Chem. A 6 (43) (2018) 21475–21484, https://doi.org/10.1039/C8TA08997C.
[53] T. Tancogne-Dejean, V. Grolleau, D. Mohr, Strain rate dependent plasticity of lithium-ion pouch cells: experiments and simulations, Int.J.Impact Eng. 159 (2022), 104048, https://doi.org/10.1016/j.ijimpeng.2021.104048.
[54] M. Raffler, W. Sinz, S. Erker, B. Brunnsteiner, C. Ellersdorfer, Influence of loading rate and out of plane direction dependence on deformation and electro-mechanical failure behavior of a lithium-ion pouch cell, J.Energy Storage 56 (2022), 105906, https://doi.org/10.1016/j.est.2022.105906.